European Radiology (2022) 32:3880–3888
https://doi.org/10.1007/s00330-021-08490-9

NUCLEAR MEDICINE

Individual [^{18}F]FDG PET and functional MRI based on simultaneous PET/MRI may predict seizure recurrence after temporal lobe epilepsy surgery

Jingjuan Wang[1] · Kun Guo[1] · Bixiao Cui[1] · Yaqin Hou[1] · Guoguang Zhao[2] · Jie Lu[1,3]

Received: 3 September 2021 / Revised: 21 October 2021 / Accepted: 28 November 2021 / Published online: 13 January 2022

Abstract

Objectives To investigate the individual measures of brain glucose metabolism, neural activity obtained from simultaneous ^{18}[F]FDG PET/MRI, and their association with surgical outcomes in medial temporal lobe epilepsy due to hippocampal sclerosis (mTLE-HS).

Methods Thirty-nine unilateral mTLE-HS patients who underwent anterior temporal lobectomy were classified as having completely seizure-free (Engel class IA; $n = 22$) or non-seizure-free (Engel class IB–IV; $n = 17$) outcomes at 1 year after surgery. Preoperative [^{18}F]FDG PET and functional MRI (fMRI) were obtained from a simultaneous PET/MRI scanner, and individual glucose metabolism and fractional amplitude of low-frequency fluctuation (fALFF) were evaluated by standardizing these with respect to healthy controls. These abnormality measures and clinical data from each patient were incorporated into a machine learning framework (gradient boosting decision tree and logistic regression analysis) to estimate seizure recurrence. The predictive values of features were evaluated by the receiver operating characteristic (ROC) curve in the training and test cohorts.

Results The machine learning classification model showed [^{18}F]FDG PET and fMRI variations in contralateral hippocampal network and age of onset identify unfavorable surgical outcomes effectively. In the validation dataset, the logistic regression model with [^{18}F]FDG PET and fALFF obtained from simultaneous [^{18}F]FDG PET/MRI gained the maximum area under the ROC curve of 0.905 for seizure recurrence, higher than 0.762 with ^{18}[F]-FDG PET, and 0.810 with fALFF alone.

Conclusion Machine learning model suggests individual [^{18}F]FDG PET and fMRI variations in contralateral hippocampal network based on ^{18}[F]-FDG PET/MRI could serve as a potential biomarker of unfavorable surgical outcomes.

Key Points

- *Individual [^{18}F]FDG PET and fMRI obtained from preoperative [^{18}F]FDG PET/MR were investigated.*
- *Individual differences were further assessed based on a seizure propagation network.*
- *Machine learning can classify surgical outcomes with 90.5% accuracy.*

Keywords Temporal lobe epilepsy · Prognosis · Metabolism · Functional magnetic resonance imaging · Machine learning

Abbreviations

[^{18}F]FDG	[^{18}F]Fluorodeoxyglucose
ALFF	Amplitude of low-frequency fluctuation
ATL	Anterior temporal lobectomy
BOLD	Blood oxygen level–dependent
GBDT	Gradient boosting decision tree
HC	Healthy control
HS	Hippocampal sclerosis
MRI	Magnetic resonance imaging
PET	Positron emission tomography
ROC	Receiver operating characteristic
SPM	Statistical parametric mapping
TLE	Temporal lobe epilepsy

Jingjuan Wang and Kun Guo contributed equally to this work.

✉ Jie Lu
imaginglu@hotmail.com

[1] Department of Radiology and Nuclear Medicine, Xuanwu Hospital Capital Medical University, Beijing 100053, China

[2] Department of Neurosurgery, Xuanwu Hospital Capital Medical University, Beijing, China

[3] Key Laboratory of Magnetic Resonance Imaging and Brain Informatics, Beijing, China

Introduction

Temporal lobe epilepsy (TLE) is the most common type of focal epilepsy, and hippocampal sclerosis (HS) is the prevalent pathological feature of mesial TLE (mTLE) [1, 2]. It is widely accepted that anterior temporal lobectomy (ATL) is an effective surgical treatment in drug-resistant mTLE-HS patients. Unfortunately, nearly 30% of patients do not achieve postoperative seizure freedom at 1 year [3, 4]. Emerging evidence indicates that the potential cause of surgical failure may be related to epileptogenic networks, which are preoperatively established and not affected during surgery, thus may provide support for seizure recurrence [5, 6]. It is important to find reliable imaging markers of epileptogenic networks to successfully predict surgical results and provide optimal therapies to improve outcomes.

Functional changes may be detected in epileptogenic networks prior to structural changes [7]. The simultaneous [^{18}F]FDG PET/MRI allows measurement of intrinsic activity and glucose metabolism at an individual level. Functional magnetic resonance imaging (fMRI) using the blood oxygenation level–dependent (BOLD) contrast indirectly probes neuronal activity change. The amplitude of low-frequency fluctuation (ALFF) of BOLD signals represents the averaged square root of the power across 0.01–0.08 Hz in a given voxel, which indirectly maps interictal epileptic activity [8]. Fractional ALFF (fALFF), the normalized index of ALFF, is known to be a more resting-specific index than ALFF [9, 10], whereas the relationship between fALFF changes in epilepsy and surgical prognosis has not been reported. Extratemporal lobe hypometabolism by [^{18}F]FDG PET is related to unfavorable surgical outcomes [11, 12]. Higo et al estimated the ratio of hypometabolism difference by three-dimensional stereotactic surface projection and reported high hypometabolism difference of "Hippocampus & Amygdala" was the most reliable prognostic factor for favorable outcomes [13]. However, its topology is highly variable across individuals, and there is no specific hypometabolic pattern that distinguishes the failures from the successful group.

Machine learning, a data analysis technique that develops algorithms to predict outcomes by learning from data, has increasingly been used in a variety of medical applications [14]. The gradient boosting decision tree (GBDT) method is a decision tree–based algorithm and could reduce the dimensionality for feature selections [15]. We hypothesized that the combination of glucose metabolism and fMRI signal abnormalities could quantify the propagation of epileptogenic activity, which may increase the predictive ability of surgical outcomes. Applying machine learning methods, we aimed to explore the relationship between presurgical [^{18}F]FDG PET and fALFF abnormalities obtained from simultaneous [^{18}F]FDG PET/MRI and surgical outcomes in mTLE-HS patients at an individual level.

Materials and methods

Participants

Thirty-nine (mean age, 27.23 ± 7.17 years, range, 14–40 years; 17 males) drug-resistant unilateral TLE-HS patients were included in the study from August 2016 to December 2018. Standard ATL was performed after comprehensive evaluations, including semiology, interictal and ictal scalp electroencephalography, MRI, [^{18}F]FDG PET/CT, simultaneous PET/MRI, and histopathological results. The ATL was performed by two experienced neurosurgeons. The mesial temporal lobe, including the ipsilateral amygdala, hippocampus, and uncinate gyrus, was resected 5.5 cm on the non-dominant hemisphere or 4.5 cm on the dominant hemisphere [16]. The inclusion criteria for patients were as follows: (1) typical symptoms of mTLE, (2) unilateral hippocampal sclerosis confirmed by histopathology, (3) epileptic spikes in the temporal lobes. Patients were excluded for (1) previous brain surgery/brain damage, (2) other chronic neurological diseases, (3) extratemporal or multifocal epilepsy, (4) TLE due to other causes, (5) TLE with crossed cerebellar diaschisis detected by [^{18}F]FDG PET, and (6) any contraindications for MRI and incomplete MRI or PET data. None of the patients had intraoperative or perioperative complications, and the preoperative antiepileptic regimen was continued for all patients in the postoperative period, with a reduction of dosage in a few patients because of their seizure freedom. No patients were excluded due to these criteria.

Seizure outcomes were categorized 1 year after surgery according to the International League Against Epilepsy (ILAE) classification scheme [17] into two groups: 22 class IA (completely seizure-free since surgery) and 17 non-class IA (including non-disabling seizures and rare/occasional seizures; defined as a suboptimal outcome [classes IB, IC, ID, and II] and failure [classes III and IV]). Such grouping methods have been used in many studies [18, 19].

For comparison, 22 age- and gender-matched healthy controls (HCs) (mean age, 29.32 ± 5.65 years, range, 17–39 years; 11 males) were recruited. All HCs were free of psychiatric or neurologic disorders on the basis of a health screening measure. This retrospective study was approved by the Ethics Committee of Xuanwu Hospital. Each subject provided written informed consent.

Interictal [^{18}F]FDG PET and MRI data were simultaneously obtained using a hybrid TOF-PET/MRI scanner

(SIGNA, GE Healthcare). MRI sequences included BOLD-fMRI and 3D T1 BRAVO images. All details about PET/MR image acquisition and data post-processing are provided in the supplementary materials.

Individual imaging analysis

Glucose metabolism and fALFF of HCs served as the normal databases. Based on the general linear model framework, individual glucose metabolism and fALFF changes were assessed by two-sample *t* tests [20, 21]. Age and gender were regressed out as covariates to reduce the effects of these variables. Intensity normalization of the cerebellum was used to estimate global effects on [^{18}F]FDG PET. fALFF maps measured the relative contribution of the low-frequency range (0.01–0.1 Hz) to the whole-frequency range of signal oscillations. A brain mask provided in DPABI (BrainMask 91*109*91) was used to obtain voxels for statistical analysis. Significance was assumed at a voxel level of $p < 0.05$ and required a minimum of 10 contiguous significant voxels. For visualization, the significant voxels were overlaid onto a high-definition T1-weighted brain template to show individual differences.

A potential seizure propagation network [22] has been identified to indicate how seizures spread from the temporal lobe to the cortex, which includes the ipsilateral subnetwork (ipsilateral hippocampus, thalamus, and insula), contralateral subnetwork (contralateral hippocampus, thalamus, and insula), and the midline subnetwork (bilateral middle cingulate and precuneus). All the individual SPM outputs in both the patient groups were randomly mixed and assessed whether the SPM outputs were involved in one of three subnetworks by two experienced neuroradiologists, and any discordance will be resolved through consultation by a third neuroradiologist. More specifically, for each patient, [^{18}F]FDG PET and fMRI variables in each subnetwork were assigned a logical value (glucose metabolism or fALFF). For instance, variables in contralateral subnetwork will be set to 1; either glucose metabolism changes or fALFF changes were involved in contralateral subnetwork; the variables in a subnetwork will be 0 if neither the two measurements change.

Feature selection and model construction

In addition to the imaging variables, six clinical variables, namely gender, age, age of onset, duration, frequency, and laterality, were also included to build the machine learning model. All patients were mixed and randomly split into a training set (70%) and a test set (30%). Before analysis, the exclusion of missing values and data standardization were done. A GBDT framework was used to extract features from clinical variables and multiparametric subnetworks. The absolute correlation threshold was set as 0.7. The selected features were used to build the logistic regression algorithm for binary classification tasks. The model was built solely with the training dataset and subsequently verified with the test dataset. The data analysis flowchart of the study is shown in Fig. 1.

Statistical analysis

All data analyses were performed with SPSS software (IBM SPSS Statistics, Version 21.0). Group-level comparisons of demographic and clinical characteristics were carried out with independent-sample *t* tests, one-way analysis of variance, or chi-square tests.

For the performance of the machine learning model, the sensitivity, specificity, accuracy, and area under the receiver operating characteristic (ROC) curve of each predictive output were calculated.

Results

Demographic and clinical characteristics

There was no significant difference between the experimental groups in age, gender, or seizure frequency ($p > 0.05$). Other clinical characteristics, including the age of onset ($p = 0.054$) and epilepsy duration ($p = 0.052$), had a marginally significant difference between the seizure-free and non-seizure-freedom groups. There is a weak significant difference in the history of medication ($p = 0.041$), as listed in Table 1.

Contralateral hippocampal network involvement related to unfavorable surgical outcomes

At the 1-year follow-up, 22 patients achieved complete seizure freedom, whereas 17 patients still had seizures. In the completely seizure-free group (Engel IA), changed glucose metabolism was presented in the ipsilateral hippocampus network of 90.9% (20/22) of patients, whereas 81.8% (18/22) showed fALFF abnormalities compared to the HCs. Only 18.2% (4/22) of patients showed involvement of the contralateral hippocampal network. [^{18}F]FDG PET detected midline network involvement in 63.6% (14/22) of patients and fALFF abnormalities in 81.8% (18/22) of patients. A representative patient whose contralateral hippocampal network was not involved is shown in Fig. 2.

In the non-seizure-freedom group (Engel IB-IV), all patients showed ipsilateral hippocampal hypometabolism, and 82.3% (14/17) of patients presented fALFF signal abnormalities in the ipsilateral hippocampal network. The contralateral hippocampal network involvement was

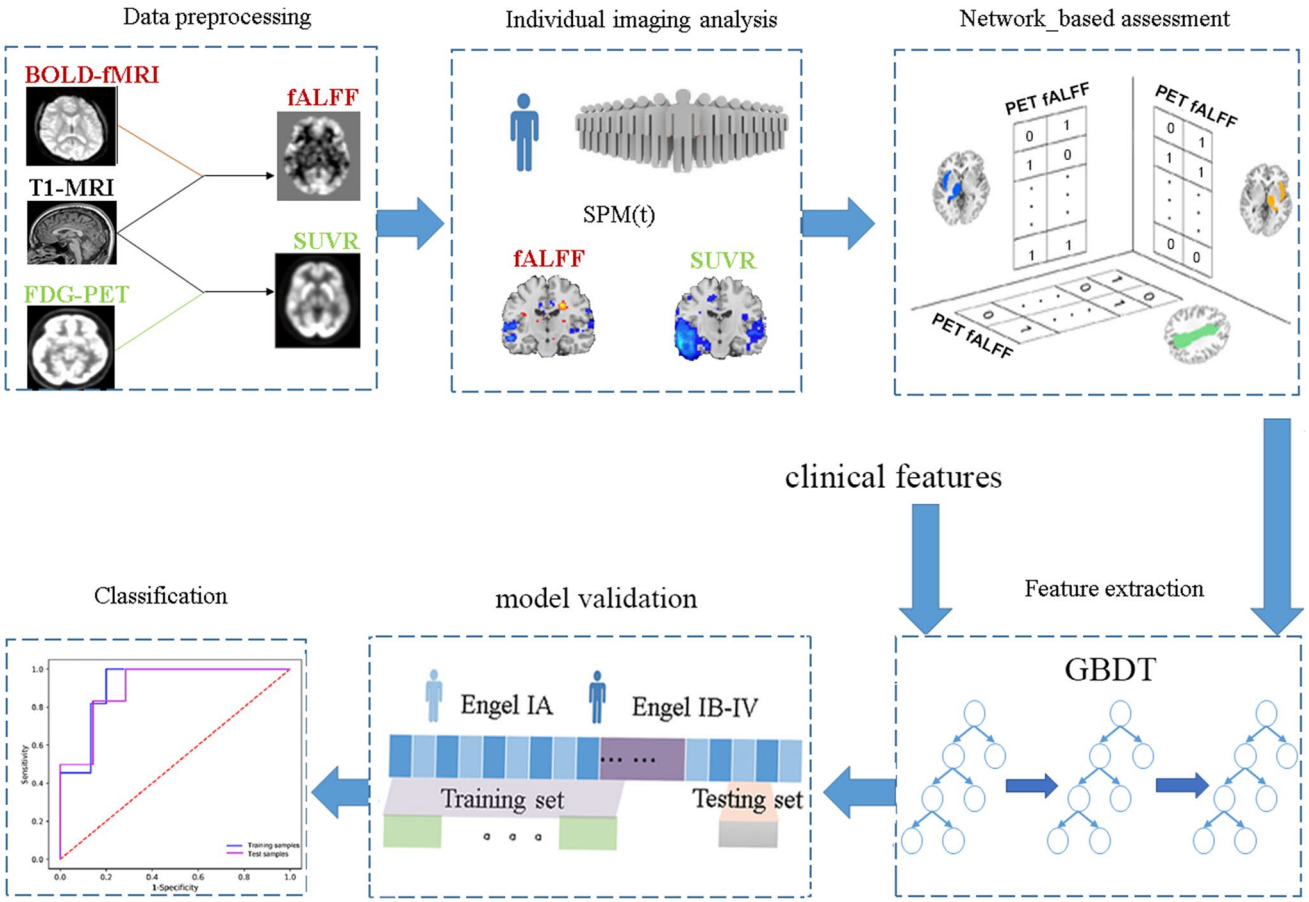

Fig. 1 Flowchart of the study. Image features from individual PET/MR imaging and clinical features were extracted. The GBDT model was applied to select two key radiomics signatures. The logistic regression model was performed to assess the predictive values of the subnetwork toward surgical outcomes. GBDT, gradient boosting decision tree

Table 1 The demographics and clinical features of all participants

Variables	Healthy controls ($N=22$)	Engel class IA ($N=22$)	Engel class IB to IV ($N=17$)[a]	p
Age, years	29.32 ± 5.79	26.86 ± 5.97	27.82 ± 7.88	0.668
Gender (M/F)	11/11	10/12	7/10	0.789
Laterality (L/R)		11/11	9/8	0.431
Age of onset, years		11.34 ± 7.68	17.06 ± 10.27	0.054
Epilepsy duration, years		10.76 ± 7.98	15.50 ± 6.74	0.052
Frequency, *n*				0.116
Daily		1	5	
Weekly		8	4	
Monthly		11	5	
Yearly		2	3	
Family history, *n*		1	0	0.373
Febrile convulsion, *n*		5	2	0.376
Viral encephalitis, *n*		4	0	0.063
Medication, *n*				0.041*
≤2		15	6	
≥3		7	11	

[a]Disease was staged as Engel class IB–D in four patients, Engel class II in eight, Engel class III in four, and Engel class IV in one. *Comparison between two patient groups, $p<0.05$

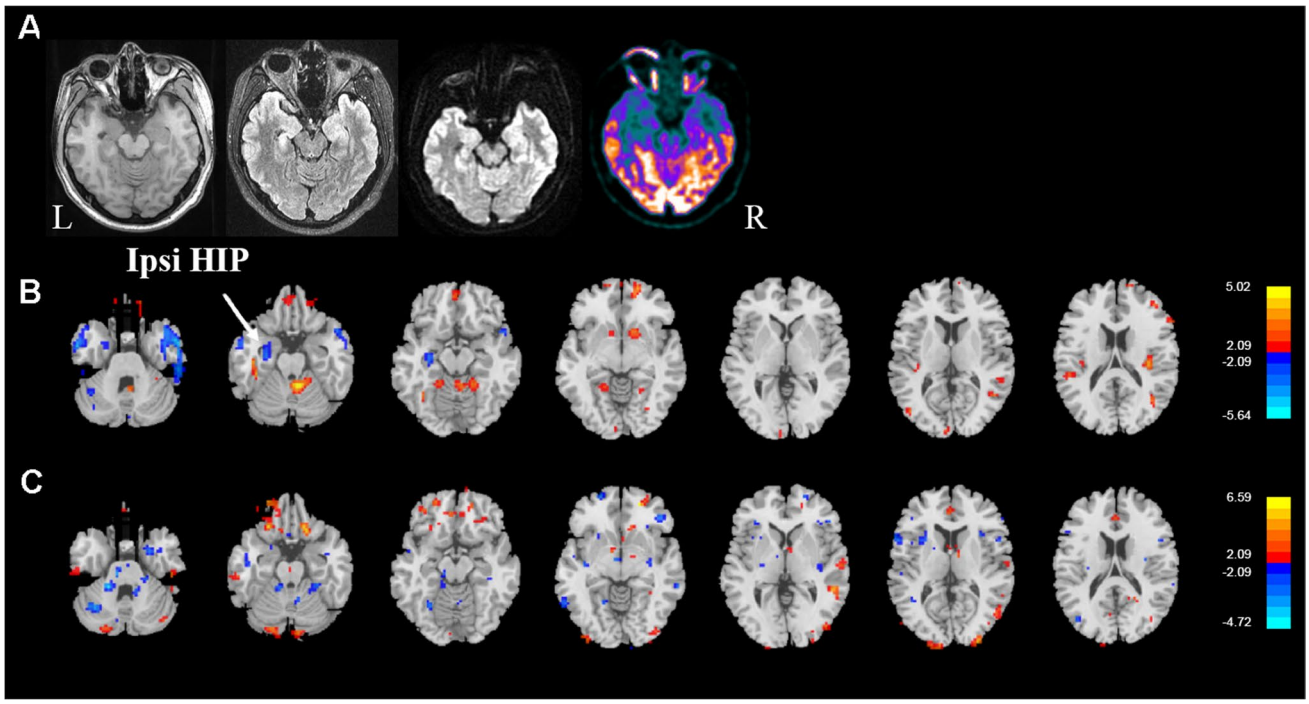

Fig. 2 A representative subject from the seizure-free group was shown. A 39-year-old female who had seizures for 18 years achieved Engel IA at the 1-year follow-up after ATL on the left side. **A** The T1-weighted images, T2 flair image, DWI image, and FDG PET image are shown from left to right. **B** Individual [^{18}F]FDG PET analysis showed that hypometabolism was distributed mainly in the left hippocampus and bilateral temporal lobe. A contralateral hippocampal network was not involved. **C** Individual BOLD-fMRI analysis showed that although increased/decreased fALFF was found in the bilateral temporal lobe and frontal lobe, the contralateral hippocampal network was not involved

detected with [^{18}F]FDG PET in 41.2% (7/17) of patients and with fALFF in 82.4% (14/17) of patients. The midline network was involved in 88.2% (15/17) of patients, which was detected by [^{18}F]FDG PET in 82.3% (14/17) of patients, and fALFF abnormalities were found in 88.2% (15/17) of patients. Figure 3 shows a representative patient in whom the contralateral hippocampal network was involved.

The number of patients whose three propagation subnetworks were involved detected by PET and fALFF is shown in Fig. 4.

Predictive values of the multiparametric subnetworks with a logistic regression model

[^{18}F]FDG PET and fMRI changes in contralateral hippocampal network and age of onset were selected by the GBDT model. The accuracy of the logistic regression model reached 80.8% across all participants. The sensitivity and specificity were 81.8% and 80.0% in the training dataset, while 100% and 71.4% in the testing dataset (Fig. 5A).

The model involving glucose metabolism and age of onset showed 54.5% sensitivity and 93.3% specificity in the training dataset, while 33.3% and 85.7% respectively in the testing dataset (Fig. 5B). The model involving fALFF and age of onset showed 72.7% sensitivity and 80.0% specificity in the training dataset, while 83.3% and 85.7% respectively in the testing dataset (Fig. 5C).

Discussion

We investigated whether individual measures of brain glucose metabolism and neural activity obtained from simultaneous [^{18}F]FDG PET/MRI could be used to predict ATL surgical outcomes. We found that the involvement of the contralateral hippocampal network detected by [^{18}F]FDG PET and fMRI abnormities had the best predictive performance for unfavorable surgical outcomes in this surgical series of patients with mTLE-HS.

There were evidences showing that the preoperative neuroimaging biomarker may be primarily associated with seizure recurrence in mTLE-HS patients [18–24]. Desalvo et al reported that lower network integration in the contralateral temporo-insular region was associated with surgical outcomes in TLE [18]. Theoretical graph measures on resting-state fMRI data revealed that thalamic "hubness" could serve as a potential biomarker of surgical outcome [23]. Sinha et al demonstrated specific structural brain network abnormalities

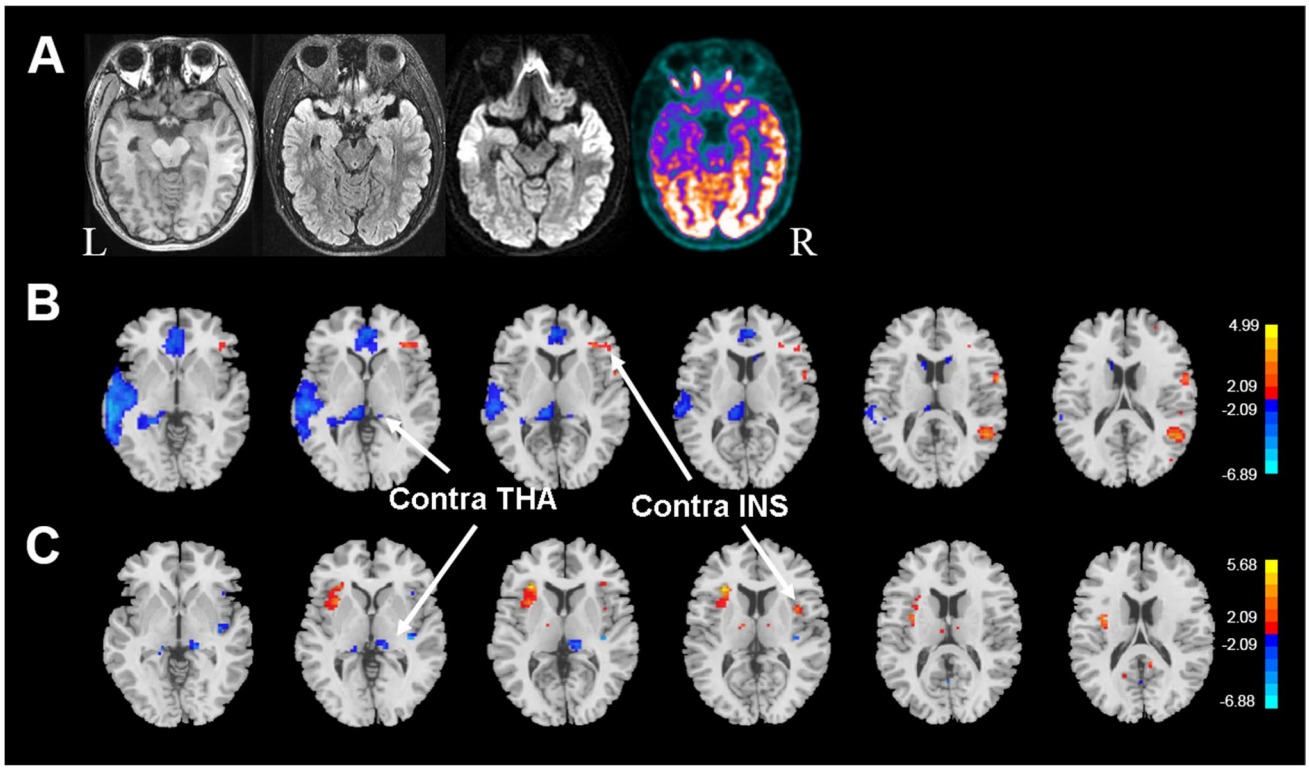

Fig. 3 A representative subject from the non-seizure-free group is shown. A 14-year-old male had seizures for 12 years and was categorized as Engel IV at the 1-year follow-up after surgery on the left side. PET/MRI showed presurgical involvement of the contralateral hippocampal network. **A** The T1-weighted images, T2 flair image, DWI image, and FDG PET image are shown from left to right. **B** Individual PET analysis showed that hypometabolism was distributed mainly in the left hippocampus, thalamus, temporal lobe, bilateral anterior cingulate cortex, and contralateral thalamus contralateral insula showing significant hypermetabolism. **C** Similar to PET result, individual BOLD-fMRI analysis showed that contralateral hippocampal network was involved, decreased fALFF in contralateral thalamus, and increased fALFF in the contralateral insula

associated with the probability of seizure recurrence following epilepsy surgery [24]. However, most studies were based on the whole brain, which might not be specific to seizure propagation. Mogan et al first proposed the seizure propagation network, including the ipsilateral hippocampal network, the midline subnetwork, and the contralateral hippocampal subnetwork [20]. The functional and structural connectivity within the seizure propagation network were further studied for epilepsy surgery outcome predictions. A critical difference in our study is that we differentiate the three subnetworks based on [^{18}F]FDG PET and fALFF measures, and potential biomarkers for seizure recurrence were also found.

A practical challenge was to identify the epileptogenic network that supports ongoing postoperative seizures. The widespread epileptogenic network appears to be related to the duration and severity of disease, and at-risk regions, supporting recurrent seizures, can differ across individual subjects. The present study investigated the seizure propagation network based on the individual level, and the results were assessed based on the three subnetworks. These results indicated that the contralateral hippocampal network involvement was associated with unfavorable prognoses, supporting the hypothesis of contralateral involvement as a potential pathophysiologic mechanism [18, 25]. Morgan et al observed a gradual increase in connection strength overtime in the bilateral hippocampus of mTLE and demonstrated that the contralateral hippocampus may begin to drive the epileptogenic hippocampus after several years of epilepsy [26]. In addition to the presumed seizure focus in the hippocampus, on preoperative resting-state functional MRI scans, lower contralateral network integration, especially involving the temporal-insula cortex, was associated with ongoing seizures in patients with temporal lobe epilepsy [18]. A thalamic network may play an important role in the secondary generalization of seizures in TLE, which may be estimated presurgically [23]. Interestingly, no matter which one of those brain regions in the contralateral hippocampal network was involved, the patients achieved unfavorable outcomes after surgery, regardless of whether the change of abnormal signal was increased or decreased. This preliminary study suggested the heterogeneity of epileptogenic networks in patients with seizure recurrence.

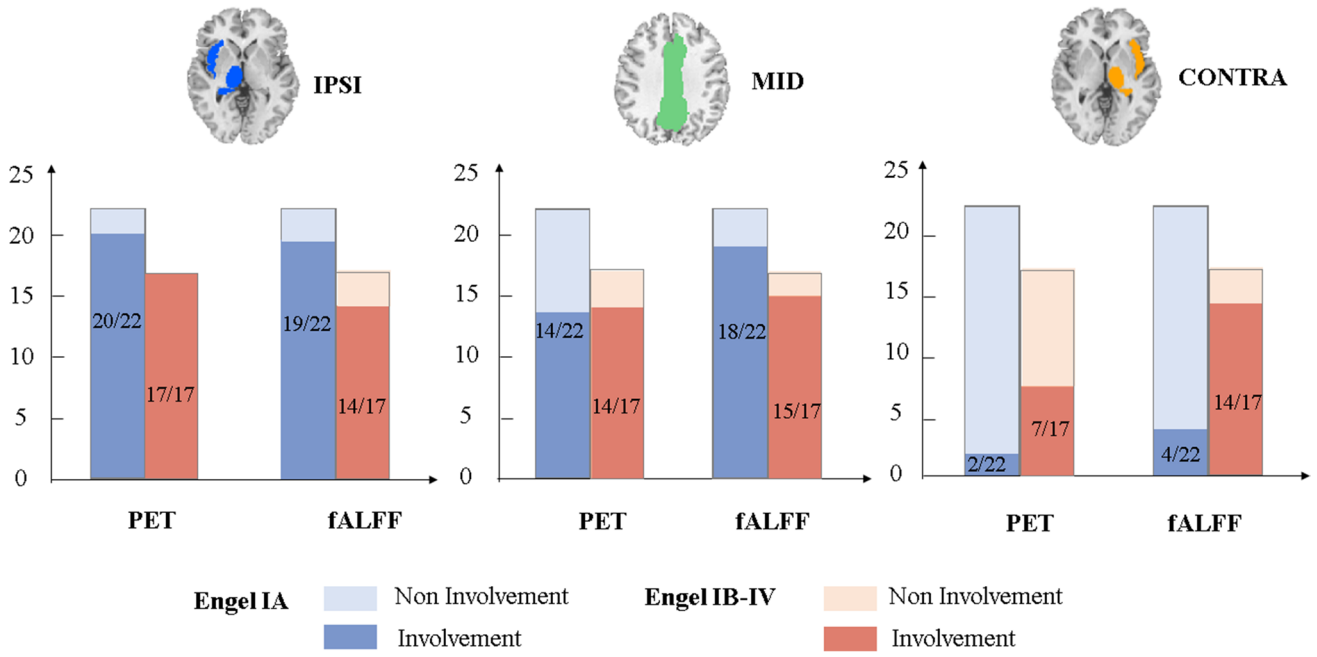

Fig. 4 Seizure propagation network properties. The network diagram shows the ipsilateral hippocampal network (IPSI, blue), midline network (MID, green), and contralateral hippocampal network (CONTRA, yellow) sets of regions. The patients were divided into completely seizure-free (Engel IA) and non-seizure-free (Engel IB-IV) groups, and the number of patients whose involvement of those three seizure subnetworks detected by PET and fALFF is shown

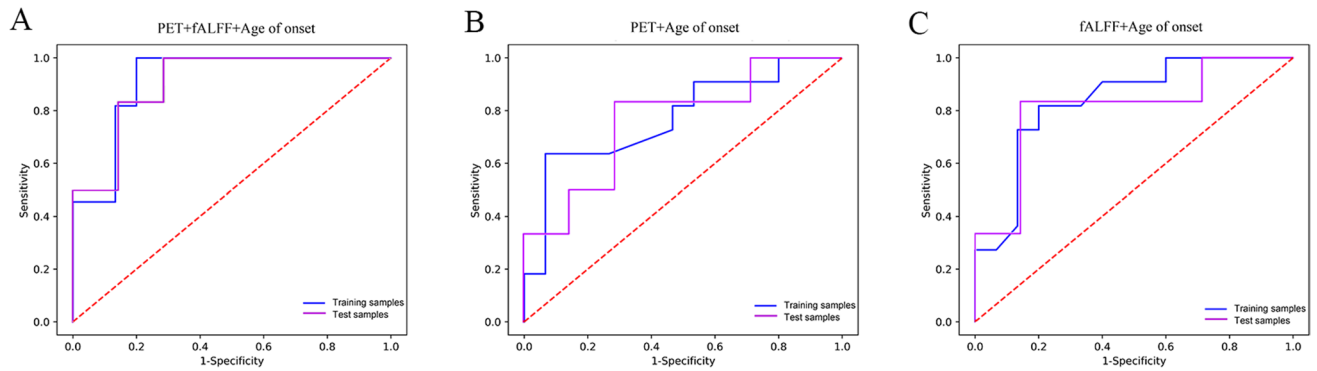

Fig. 5 ROC curves of features in the training and test cohorts. AUC was 0.915 and 0.905 in the training and test cohorts for models that included multiparametric imaging in the contralateral hippocampal network and age of onset; AUC was 0.773 and 0.762 in the training and test cohorts for models that included individual glucose metabolism imaging in the contralateral hippocampal network and age of onset; AUC was 0.836 and 0.810 in the training and test cohorts for models that included individual fALFF change in the contralateral hippocampal network and age of onset. ROC, receiver operating characteristic; AUC, the area under ROC curve

In practice, it is difficult for clinicians to visually identify the hypermetabolism in the hypermetabolic background, but the mirror hypermetabolism was grossly proportional to the hypometabolic areas [27], which is consistent with our results. Similar to glucose metabolism changes, fALFF analysis based on functional MRI may be contaminated by confounding factors, including head motion, physiologic interference (cardiac pulse and respiration), and hardware artifacts [28]. The fALFF has been extensively applied in epilepsy studies and is thought to affect epileptic discharges [29]. Data of simultaneous EEG-fMRI suggested that the ALFF abnormalities might be associated with interictal epileptiform discharges [30, 31].

In the present study, our results add to the growing evidence supporting the utility of simultaneous PET/MRI in the presurgical evaluation of patients with TLE, particularly as a prognostic tool to predict surgical outcomes. A few studies have investigated the relationship between

surgical outcomes and the combination of PET and other functional parameters [32, 33]. This current study further investigated the potential personalized biomarker of multiparametric imaging abnormalities, including PET and fALFF, and machine learning models were applied in the prediction of surgical outcomes in epilepsy. The GBDT, an optimal feature selection method, was used to select optimal features from clinical features and PET/MRI data. The classification method option is the most prominent cause of performance variation, and feature selection strategies could increase the generalizability of models. Through the evaluation of five feature selection methods and nine classification methods, Zhou et al found GBDT was considered the optimal feature selection method for the PET dataset [34]. In this study, the model with multiparametric imaging and age of onset had the best predictive performance for unfavorable outcomes on the individual level. We found the model with [^{18}F]FDG PET, fMRI, and age of onset had the strongest predictive value than single imaging, indicating that multiparametric imaging had a powerful predictive value for unfavorable outcomes on an individual level. Accordingly, our study is an important step toward implementing multiparametric imaging from PET/MR in the prediction of postsurgical outcomes in mTLE-HS, potentially improving patient selection and counseling.

An important limitation of this study was the relatively small sample size in the unfavorable outcome group and the nature of retrospective studies. However, it was believed that the homogeneity in the sample recruitment allowed a better comprehension of the abnormalities found in PET and fMRI in patients with mTLE-HS using a hybrid PET/MRI scanner. It is notable that the present study provides empirical evidence of the clinical utility of hybrid PET/MRI data in predicting surgical outcomes following epilepsy surgery. In addition, we only studied fALFF in a single conventional frequency range (0.01 to 0.1 Hz). Previous studies have shown that alpha waves are abnormal in epilepsy [35], and the frequency range of 73–198 mHz (slow-3 sub-band) appeared to be the most helpful in distinguishing patients with new-onset from first-seizure ones [27]. Though the frequency range in our study overlapped most parts of the slow-3 sub-band, more specific frequency bands might need to be considered. Finally, changes in signals might carry important physiological information. However, we did not categorize signals into rising or decreasing groups in this study. In the future study, we would respectively investigate the potential physiological information of signal spikes and declines based on a larger sample size.

In summary, the findings of this study suggest that preoperative multiparametric imaging involving the contralateral hippocampal network is associated with unfavorable postoperative surgical outcomes in TLE-HS patients.

Supplementary Information The online version contains supplementary material available at https://doi.org/10.1007/s00330-021-08490-9.

Acknowledgements The authors thank the clinical scientists Hong Li and Yuchao Xu from GE Healthcare for their suggestions to improve this manuscript.

Funding This study was supported by the Project of Beijing Municipal Administration of Hospitals' Ascent Plan, Code: DFL 20180802.

Declarations

Guarantor The scientific guarantor of this publication is Jie Lu.

Conflict of interest The authors of this manuscript declare no relationships with any companies whose products or services may be related to the subject matter of the article.

Statistics and biometry No complex statistical methods were necessary for this paper.

Informed consent Written informed consent was obtained from all subjects (patients) in this study.

Ethical approval Institutional Review Board approval was obtained.

Methodology
- retrospective
- diagnostic or prognostic study
- performed at one institution

References

1. Rodriguez-Cruces R, Bernhardt BC, Concha L (2020) Multidimensional associations between cognition and connectome organization in temporal lobe epilepsy. Neuroimage 213:116706. https://doi.org/10.1016/j.neuroimage.2020.116706
2. Li W, Jiang Y, Qin Y et al (2021) Structural and functional reorganization of contralateral hippocampus after temporal lobe epilepsy surgery. Neuroimage Clin 31:102714. https://doi.org/10.1016/j.nicl.2021.102714
3. Thijs RD, Surges R, O'Brien TJ, Sander JW (2019) Epilepsy in adults. Lancet 393:689–701. https://doi.org/10.1016/S0140-6736(18)32596-0
4. Pitkanen A, Loscher W, Vezzani A et al (2016) Advances in the development of biomarkers for epilepsy. Lancet Neurol 15:843–856. https://doi.org/10.1016/S1474-4422(16)00112-5
5. Grobelny BT, London D, Hill TC, North E, Dugan P, Doyle WK (2018) Betweenness centrality of intracranial electroencephalography networks and surgical epilepsy outcome. Clin Neurophysiol 129:1804–1812. https://doi.org/10.1016/j.clinph.2018.02.135
6. Andrews JP, Gummadavelli A, Farooque P et al (2019) Association of seizure spread with surgical failure in epilepsy. JAMA Neurol 76:462–469. https://doi.org/10.1001/jamaneurol.2018.4316
7. O'Muircheartaigh J, Vollmar C, Barker GJ et al (2012) Abnormal thalamocortical structural and functional connectivity in juvenile myoclonic epilepsy. Brain 135:3635–3644. https://doi.org/10.1093/brain/aws296

8. Zhang Z, Lu G, Zhong Y et al (2010) fMRI study of mesial temporal lobe epilepsy using amplitude of low-frequency fluctuation analysis. Hum Brain Mapp 31:1851–1861. https://doi.org/10.1002/hbm.20982
9. Zou QH, Zhu CZ, Yang Y et al (2008) An improved approach to detection of amplitude of low-frequency fluctuation (ALFF) for resting-state fMRI: fractional ALFF. J Neurosci Methods 172:137–141. https://doi.org/10.1016/j.jneumeth.2008.04.012
10. Hwang G, Nair VA, Mathis J et al (2019) Using low-frequency oscillations to detect temporal lobe epilepsy with machine learning. Brain Connect 9:184–193. https://doi.org/10.1089/brain.2018.0601
11. Tomas J, Pittau F, Hammers A et al (2019) The predictive value of hypometabolism in focal epilepsy: a prospective study in surgical candidates. Eur J Nucl Med Mol Imaging 46:1806–1816. https://doi.org/10.1007/s00259-019-04356-x
12. Cahill V, Sinclair B, Malpas CB et al (2019) Metabolic patterns and seizure outcomes following anterior temporal lobectomy. Ann Neurol 85:241–250. https://doi.org/10.1002/ana.25405
13. Higo T, Sugano H, Nakajima M et al (2016) The predictive value of FDG-PET with 3D-SSP for surgical outcomes in patients with temporal lobe epilepsy. Seizure 41:127–133. https://doi.org/10.1016/j.seizure.2016.07.019
14. Abbasi B, Goldenholz DM (2019) Machine learning applications in epilepsy. Epilepsia 60:2037–2047. https://doi.org/10.1111/epi.16333
15. An Q, Yu L(2021) A heterogeneous network embedding framework for predicting similarity-based drug-target interactions. Brief Bioinform. bbab275. https://doi.org/10.1093/bib/bbab275
16. Wang YH et al (2018) Comparison between simultaneously acquired arterial spin labeling and [^{18}F]FDG PET in mesial temporal lobe epilepsy assisted by a PET/MR system and SEEG. Neuroimage Clin 19:824–830. https://doi.org/10.1016/j.nicl.2018.06.008
17. Scheffer IE, Berkovic S, Capovilla G et al (2017) ILAE classification of the epilepsies: position paper of the ILAE Commission for Classification and Terminology. Epilepsia 58:512–521. https://doi.org/10.1111/epi.13709
18. DeSalvo MN, Tanaka N, Douw L, Cole AJ, Stufflebeam SM (2020) Contralateral preoperative resting-state functional MRI network integration is associated with surgical outcome in temporal lobe epilepsy. Radiology 294:622–627. https://doi.org/10.1148/radiol.2020191008
19. Job AS, David O, Minotti L, Bartolomei F, Chabardes S, Kahane P (2019) Epileptogenicity maps of intracerebral fast activities (60–100 Hz) at seizure onset in epilepsy surgery candidates. Front Neurol 10:1263. https://doi.org/10.3389/fneur.2019.01263
20. Lagarde S, Boucekine M, McGonigal A et al (2020) Relationship between PET metabolism and SEEG epileptogenicity in focal lesional epilepsy. Eur J Nucl Med Mol Imaging 47:3130–3142. https://doi.org/10.1007/s00259-020-04791-1
21. Lin Y, Fang YD, Wu G et al (2018) Quantitative positron emission tomography-guided magnetic resonance imaging postprocessing in magnetic resonance imaging-negative epilepsies. Epilepsia 59:1583–1594. https://doi.org/10.1111/epi.14474
22. Morgan VL, Englot DJ, Rogers BP et al (2017) Magnetic resonance imaging connectivity for the prediction of seizure outcome in temporal lobe epilepsy. Epilepsia 58:1251–1260. https://doi.org/10.1111/epi.13762
23. He X, Doucet GE, Pustina D, Sperling MR, Sharan AD, Tracy JI (2017) Presurgical thalamic "hubness" predicts surgical outcome in temporal lobe epilepsy. Neurology 88:2285–2293. https://doi.org/10.1212/WNL.0000000000004035
24. Sinha N, Wang Y, Moreira da Silva N et al (2021) Structural brain network abnormalities and the probability of seizure recurrence after epilepsy surgery. Neurology 96:e758–e771. https://doi.org/10.1212/WNL.0000000000011315
25. Bettus G, Guedj E, Joyeux F et al (2009) Decreased basal fMRI functional connectivity in epileptogenic networks and contralateral compensatory mechanisms. Hum Brain Mapp 30:1580–1591. https://doi.org/10.1002/hbm.20625
26. Morgan VL, Abou-Khalil B, Rogers BP (2015) Evolution of functional connectivity of brain networks and their dynamic interaction in temporal lobe epilepsy. Brain Connect 5:35–44. https://doi.org/10.1089/brain.2014.0251
27. Chassoux F, Artiges E, Semah F et al (2016) Determinants of brain metabolism changes in mesial temporal lobe epilepsy. Epilepsia 57:907–919. https://doi.org/10.1111/epi.13377
28. Jo HJ, Reynolds RC, Gotts SJ et al (2020) Fast detection and reduction of local transient artifacts in resting-state fMRI. Comput Biol Med 120:103742. https://doi.org/10.1016/j.compbiomed.2020.103742
29. Gupta L, Janssens R, Vlooswijk MC et al (2017) Towards prognostic biomarkers from BOLD fluctuations to differentiate a first epileptic seizure from new-onset epilepsy. Epilepsia 58:476–483. https://doi.org/10.1111/epi.13658
30. Liao W, Zhang Z, Pan Z et al (2011) Default mode network abnormalities in mesial temporal lobe epilepsy: a study combining fMRI and DTI. Hum Brain Mapp 32:883–895. https://doi.org/10.1002/hbm.21076
31. Xu Q, Hu Z, Yang F et al (2020) Resting state signal latency assesses the propagation of intrinsic activations and estimates anti-epileptic effect of levetiracetam in Rolandic epilepsy. Brain Res Bull 162:125–131. https://doi.org/10.1016/j.brainresbull.2020.05.016
32. Shang K, Wang J, Fan X et al (2018) Clinical value of hybrid TOF-PET/MR imaging-based multiparametric imaging in localizing seizure focus in patients with MRI-negative temporal lobe epilepsy. AJNR Am J Neuroradiol 39:1791–1798. https://doi.org/10.3174/ajnr.A5814
33. Wang J, Shan Y, Dai J et al (2020) Altered coupling between resting-state glucose metabolism and functional activity in epilepsy. Ann Clin Transl Neurol 7:1831–1842. https://doi.org/10.1002/acn3.51168
34. Zhou Y, Ma X-L, Zhang T et al (2021) Use of radiomics based on 18F-FDG PET/CT and machine learning methods to aid clinical decision-making in the classification of solitary pulmonary lesions: an innovative approach. Eur J Nucl Med Mol Imaging 48:2904–2913. https://doi.org/10.1007/s00259-021-05220-7
35. Halgren M, Ulbert I, Bastuji H et al (2019) The generation and propagation of the human alpha rhythm. Proc Natl Acad Sci U S A 116:23772–23782. https://doi.org/10.1073/pnas.1913092116